

SI Appendix

1. PCR primers used in promoter construction

The newly designed promoters used in this study are listed in Table S1 (see also Fig. 1).

Promoter D12 was constructed previously (1).

Promoter	Template	Reaction	Upstream Fragment Primers	Downstream Fragment Primers
S1	pESC-LEU	1	TCCTCGTCTT ACCGGTC	GAGA ACTTTCAACATTTTCGGTTTGATTAC
			GGGA CAGTTTTTGCATTTATATATCTG	CTAGCCGC GCTACCAAGCTTAC
	Product 1	2	TCCTCGTCTT ACCGGTC	5'-P- TGATAGAGA ACTTTCAACATTTTCGGTTTG
			5'-P- CTGATAGGGA CAGTTTTTGCATTTATATATC	CTAGCCGC GCTACCAAGCTTAC
S2	pESC-LEU	1	TCCTCGTCTT ACCGGTC	GAGAT ATTACTTCTTATTCAAATGTAATAAAAAG
			GGGAG TATTAGTTAAAGTGTTATG	CTAGCCGC GCTACCAAGCTTAC
	Product 1	2	TCCTCGTCTT ACCGGTC	5'-P- TGATAGAGA TATTACTTCTTATTCAAATGTAATAAAAAG
			5'-P- CTGATAGGGA GTATTAGTTAAAGTGTTATG	CTAGCCGC GCTACCAAGCTTAC
S3	pESC-LEU	1	TCCTCGTCTT ACCGGTC	GAGA AGTATCAACAAAAAATTGTTAATATACCTCTATAC
			GGGAA AGTAATACAAACCGAAAAATGTTG	CTAGCCGC GCTACCAAGCTTAC
	Product 1	2	TCCTCGTCTT ACCGGTC	5'-P- TGATAGAGA AGTATCAACAAAAAATTGTTAATATACCTC
			5'-P- CTGATAGGGA AGTAATACAAACCGAAAAATG	CTAGCCGC GCTACCAAGCTTAC
D13	S1	1	CCGCCCTTTAGTGAGGGT TGAATTCG	GAGA AGTATCAACAAAAAATTGTTAATATACCTCTATAC
			GGGAA AGTAATACAAACCGAAAAATGTTG	CTAGCCGC GCTACCAAGCTTAC
	Product 1	2	CCGCCCTTTAGTGAGGGT TGAATTCG	5'-P- TGATAGAGA AGTATCAACAAAAAATTGTTAATATACCTC
			5'-P- CTGATAGGGA AGTAATACAAACCGAAAAATG	CTAGCCGC GCTACCAAGCTTAC
D23	S2	1	TCCTCGTCTT ACCGGTC	GAGA AGTATCAACAAAAAATTGTTAATATACCTCTATAC
			GGGAA AGTAATATCTCTATCACTG	CTAGCCGC GCTACCAAGCTTAC
	Product 1	2	TCCTCGTCTT ACCGGTC	5'-P- TGATAGAGA AGTATCAACAAAAAATTGTTAATATACCTC
			5'-P- CTGATAGGGA AGTAATATCTCTATCACTG	CTAGCCGC GCTACCAAGCTTAC
T123	D12	1	CCGCCCTTTAGTGAGGGT TGAATTCG	GAGA AGTATCAACAAAAAATTGTTAATATACCTCTATAC
			GGGAA AGTAATATCTCTATCACTG	CTAGCCGC GCTACCAAGCTTAC
	Product 1	2	CCGCCCTTTAGTGAGGGT TGAATTCG	5'-P- TGATAGAGA AGTATCAACAAAAAATTGTTAATATACCTC
			5'-P- CTGATAGGGA AGTAATATCTCTATCACTG	CTAGCCGC GCTACCAAGCTTAC
S2palindrome	pESC-LEU	1	CCGCCCTTTAGTGAGGGT TGAATTCG	AGCT TATTACTTCTTATTCAAATG
			AGCT GATTAGTTAAAGTGTTATGC	AAT AGGATCC GGGGTTTTTCTCCTTG
	Product 1	2	CCGCCCTTTAGTGAGGGT TGAATTCG	5'-P- GACTGAGCT TATTACTTCTTATTCAAATG
			5'-P- CGACTGAGCT GATTAGTTAAAGTGTTATGC	AAT AGGATCC GGGGTTTTTCTCCTTG
S2random	pESC-LEU	1	CCGCCCTTTAGTGAGGGT TGAATTCG	CGCA TATTACTTCTTATTCAAATG
			TATCG TATTAGTTAAAGTGTTATGC	AAT AGGATCC GGGGTTTTTCTCCTTG
	Product 1	2	CCGCCCTTTAGTGAGGGT TGAATTCG	5'-P- GCTATCGCA TATTACTTCTTATTCAAATG
			5'-P- GCGTGCTAT CGTATTAGTTAAAGTGTTATGC	AAT AGGATCC GGGGTTTTTCTCCTTG

Table S1. PCR primers used in promoter construction. Each promoter is listed in the far left column (see Fig. 1). This is followed by the template used in each indicated PCR reaction in the next two columns. Plasmid pESC-LEU (Stratagene) contained the wild-type *GAL1* promoter sequence. Primers used to insert *tetO₂* operator sites in different locations in the *GAL1* promoter are listed for both the upstream and downstream fragments, which were ligated together following PCR reaction 2 into plasmid pRS4D1 backbone. All primer sequences are in 5' to 3' orientation. Forward primers are listed

Figure S1. General scheme for modeling the single and multiple operator-containing promoters.

In the steady-state approximation, based on mass-action kinetics and detailed balance, the following set of equations describes the system shown in Fig. S1 ($i = 1, 2$ or 3 corresponds to promoter S_i):

$$N_i^{\&} = -r_i N_i + \rho_i R_i - a_i N_i + \alpha_i A_i = 0 \quad (\text{S1})$$

$$R_i^{\&} = r_i N_i - \rho_i R_i = 0 \quad (\text{S2})$$

$$A_i^{\&} = a_i N_i - \alpha_i A_i = 0 \quad (\text{S3})$$

$$M_i^{\&} = \lambda_i R_i + m A_i - \mu M_i = 0 \quad (\text{S4})$$

$$P_i^{\&} = p M_i - \pi P_i = 0 \quad (\text{S5})$$

Most rates in the model were assumed to be independent of the inducer concentration I , except the rates of transition between states N_i and R_i and the basal expression rate λ_i . Specifically, we assumed that the de-repression rate ρ_i (from state R_i to state N_i) depends on the concentration of inducer I as

$$\rho_i = k_i^- I^{n_i}, \quad (\text{S6})$$

because inducer molecules relieve repression by associating with DNA-bound TetR (2). The inducer molecules can also bind to free repressors, reducing their number according to the equation

$$F(I) = \frac{T}{f(I)}, \quad (\text{S7})$$

where T is the total repressor concentration, while $f(I) = 1 + I + I^2$. Therefore, the repression rate r_i (from state N_i to state R_i) depends on the concentration of free repressor F as

$$r_i = k_i^+ F_i(I) = \frac{k_i^+ T}{f(I)}. \quad (\text{S8})$$

Using Eqs. **S1-S5**, we calculated the equilibrium protein concentration, which depends on the concentration of the promoter states A_i and R_i from which mRNA is created:

$$P_i = \frac{P}{\pi\mu} (mA_i + \lambda_i R_i). \quad (\text{S9})$$

In Equation (S9), $\lambda_i = \Lambda_i(1 + L_i I)$ describes the basal expression from the repressed state R_i . After using the constraint $R_i + N_i + A_i = D$ (i.e., the total DNA concentration is constant), the concentration of promoter states can be calculated as

$$A_i = \frac{a_i}{\alpha_i} \left/ \left(\frac{r_i}{\rho_i} + 1 + \frac{a_i}{\alpha_i} \right) \right., \quad N_i = 1 \left/ \left(\frac{r_i}{\rho_i} + 1 + \frac{a_i}{\alpha_i} \right) \right., \quad R_i = \frac{r_i}{\rho_i} \left/ \left(\frac{r_i}{\rho_i} + 1 + \frac{a_i}{\alpha_i} \right) \right. . \quad (\text{S10})$$

For simplicity, we assume $D = 1$. From here, the protein concentration is:

$$P_i = \frac{p}{\pi\mu} \left(\frac{ma_i}{\alpha_i} + \frac{\lambda_i r_i}{\rho_i} \right) \left/ \left(\frac{r_i}{\rho_i} + 1 + \frac{a_i}{\alpha_i} \right) \right. . \quad (\text{S11})$$

At full induction, none of the repressor molecules are free, and therefore the repression rate $r_i \approx 0$. This implies that the protein concentration at full induction is

$$P_i^{\max} = \frac{P}{\pi} \left(\frac{m}{\mu} \frac{a_i}{a_i + \alpha_i} \right). \quad (\text{S12})$$

The rates of transition between states N_i and A_i , a_i and α_i , varied from promoter to promoter, to reflect the differences in protein expression at maximum induction (P_i^{\max}). Our experiments indicate that repressor binding does not contribute to protein expression at maximum induction (see the main text). Therefore, we attributed these differences to the sequence-dependent binding efficiency of general transcription factors and preinitiation complex (PIC) assembly.

At full repression ($I = 0$), we have $\rho_i = 0$. Therefore, the equilibrium protein concentration at full repression is

$$P_i^{\min} = \frac{P}{\pi} \frac{\Lambda_i}{\mu}. \quad (\text{S13})$$

Finally, after introducing the notation $v_i = n_i \sqrt{\frac{k_i^-}{k_i^+} \left(1 + \frac{a_i}{\alpha_i} \right)}$, we obtain the protein

concentration P_i :

$$P_i = \frac{P_i^{\max} \left(1 + \frac{a_i}{\alpha_i} \right) + P_i^{\min} \frac{k_i^+ (1 + L_i I)}{k_i^- I^{n_i} f_i(I)}}{\frac{k_i^+}{k_i^- I^{n_i} f_i(I)} + 1 + \frac{a_i}{\alpha_i}} = \frac{P_i^{\max} (v_i I)^{n_i} f_i(I) + P_i^{\min} (1 + L_i I)}{(v_i I)^{n_i} f_i(I) + 1}. \quad (\text{S14})$$

According to these calculations, the the fitting parameters v_i , L_i and n_i relate to the inducer concentration I , the total repressor concentration T and the kinetic parameters shown in Fig. S1 (and in Fig. 3 in the main text) as:

$$v_i = \sqrt[n_i]{\frac{\rho_i}{r_i} \left(1 + \frac{a_i}{\alpha_i}\right) \frac{T}{f_i(I) I^{n_i}}}, \text{ or } \frac{\rho_i}{r_i} \left(1 + \frac{a_i}{\alpha_i}\right) = \frac{(Iv_i)^{n_i} f_i(I)}{T}; \text{ (S15)}$$

$$L_i = \frac{1}{I} \left(\frac{p\lambda_i}{\mu\pi P_i^{\min}} - 1 \right) \text{ or } \lambda_i = \frac{\mu\pi P_i^{\min}}{p} (1 + L_i I); \text{ (S16)}$$

$$n_i = \ln \left(\frac{\rho_i}{k_i^-} \right) / \ln(I) \text{ or } \rho_i = k_i^- I^{n_i}. \text{ (S17)}$$

The parameters v_i and n_i together determine the inducibility of the promoter (the response of the promoter to intermediate inducer concentrations). Theoretically, n_i represents the number of inducer molecules necessary to relieve repression. The parameter L_i determines the slope of the dose-response curve at low levels of induction.

Admittedly, we were unable to assign a mechanistic, molecular-level interpretation to our fitting parameters. Because the TetR repressor can accommodate the binding of a maximum of two inducer molecules, the high slope of the dose-response curve (Hill coefficient $h = 6.67$, see Table S2) that decreases as a single repressor site is moved away from the TATA box is inconsistent with two or one inducer molecules relieving repression. Similarly, the Hill coefficient of the promoter D12 was too high ($h = 11.13$, see Table S2) to allow for a molecular-level interpretation. The maximum Hill coefficient consistent with a single repressor binding site is $h = 4$, while the maximum Hill coefficient consistent with two repressor sites is $h = 8$.

3. Parameters used in the generic model

We assigned generic values available from the literature to a subset of our parameters, as follows:

$m = 10.0$, rate of transcription initiation in galactose-grown yeast (3);

$\mu = \ln(2)/1$, rate of mRNA degradation (3);

$P = 1$, translation rate;

$\pi = \ln(2)/180$, protein degradation rate;

$$a/\alpha = \alpha_i P_i^{\max} / \left(\frac{mp}{\mu\pi} - P_i^{\max} \right), \text{ equilibrium constant of promoter activation (4, 5).}$$

In our simulations, we considered the average yeast cell volume, $50 \mu\text{m}^3$ (6), as a unit. Therefore, with appropriate choice of units, concentrations become equivalent to copy numbers per cell, and reaction rates become numerically equal to reaction probabilities per unit time (7). Although time is measured in “arbitrary units”, the known reaction rates are approximately set to their values in minutes, so the time scale for all of the resulting dynamics might be interpreted approximately in minutes.

The expression (S14) contains three unknown parameters — v_i , L_i and n_i — that were estimated by nonlinear minimization using the Nelder-Mead algorithm (fminsearch, Matlab) and the maximum and minimum expression levels (P^{\max} and P^{\min}) for each of our eight promoters (Table S2).

	WT	S1	S2	S3	D12	D13	D23	T123
P^{\max}	1458±25	1461±22	855±10	1694±33	1039±64	1565±124	1235±68	1357±29
P^{\min}	1458±25	21.2±0.5	50±2	637±22	6.29± 0.01	18±1.2	76±2.4	3.58±0.09
v	N/A	0.0091	0.0042	0.0043	0.0111	0.0118	0.0073	0.0073
L	N/A	0.0556	0.0310	0.0312	0.0077	0.0579	0.0328	0.0211
n	N/A	6.4451	4.1577	3.1855	9.7572	7.8272	5.6028	5.5897

Table S2. Parameters used in modeling the promoters WT, S1, S2, S3, D12, D13, D23 and T123.

Using a terminology adapted from Hill functions, the parameters v_i and n_i together determine the induction threshold and slope of the dose-response function at high levels of induction, while L_i determines the slope of the dose-response function at low induction, due to basal expression from the repressed promoter state (Fig. S2).

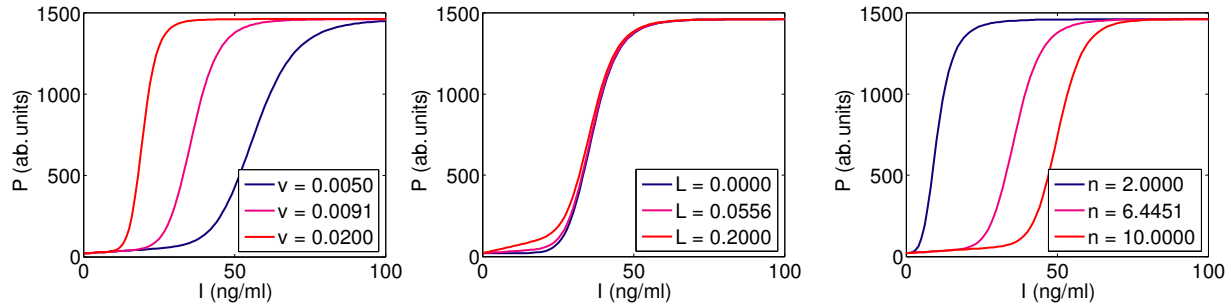


Figure S2. The effect of the parameters v_i , L_i and n_i on the dose-response function. The magenta line corresponds to the parameters used to fit the experimental data from promoter S1.

4. Stochastic simulation of promoter dynamics

We applied stochastic simulations to model the dynamics of the P_{GALI^*} promoter, using a Perl wrapper written around the software Dizzy (8), setting the extracellular anhydrotetracycline (ATc) concentration to the desired value. We allowed the system to reach steady state and estimated the mean, standard deviation and noise over a long time-course (50000 time units). We then calculated the error in the mean, standard deviation and noise by repeating the simulation ten times. We chose to estimate the mean, standard deviation and noise over a long time-course (instead of over a population), assuming that the modeled processes are ergodic. To verify the ergodicity of the process, we also calculated the mean, standard deviation and noise over a population of 100 cells in steady state. The values we estimated over a single time-course did not differ from the values obtained over a population, validating our approach.

Modeling gene expression noise by stochastic simulations requires additional parameters (actual reaction rates) compared to modeling the dose-response curve (which can be

analytically calculated from equilibrium constants). Below we show the actual transition rates between promoter states $N \leftrightarrow A$ and $N \leftrightarrow R$ that we used in all of our stochastic simulations, after estimating the scaling factors ($s_A = 0.25$ and $s_R = 50$) from the experimentally measured noise of the promoters WT and S1, respectively:

$\alpha = 0.25$, rate of promoter activation (4);

$$a = \alpha_i P_i^{\max} \left/ \left(\frac{mp}{\mu\pi} - P_i^{\max} \right) \right., \text{ rate of promoter de-activation (5);}$$

$r = 50/(1 + I + I^2)$, rate of repression; and

$$\rho = 50(v_i I)^{n_i} \left/ \left(1 + \frac{a_i}{\alpha_i} \right) \right., \text{ rate of de-repression.}$$

5. Predictability of dose-response and noise of the multiple operator-containing promoters

To address the question whether multiple multiple operator-containing promoters are predictable based on single operator-containing promoters, we replaced the state R (see Fig. S1) with multiple repressed states, according to the number of repressors bound to the promoter in various positions. We quantified predictability by calculating the Euclidian distance between the experimental data and the theoretical fit. Using the generic model (Fig. S1), the distances between the experimental data and the theoretical fit were 0.5315, 0.2875, 0.1268, and 0.2014 for promoters D12, D13, D23 and T123, respectively.

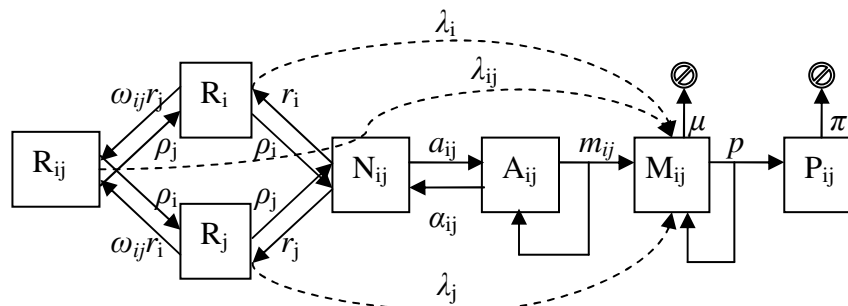


Figure S3: Chemical reaction scheme for modeling the double operator-containing promoter D_{ij} .

For a double operator-containing promoter D_{ij} , three repressed states are possible (Fig. S3): two with each of the repressor bound individually (R_i and R_j), and one with both repressors bound (R_{ij}). Based on chemical mass action and detailed balance, protein expression from the promoter D_{ij} can be calculated as follows.

$$R_i^{\&} = r_i N_{ij} - \rho_i R_i - \omega_{ij} r_j R_i + \rho_j R_{ij} = 0 \Rightarrow R_i = \frac{r_i}{\rho_i} N_{ij}; R_j = \frac{r_j}{\rho_j} N_{ij} \quad (\text{S18})$$

$$R_{ij}^{\&} = \omega_{ij} r_i R_j - \rho_i R_{ij} + \omega_{ij} r_j R_i - \rho_j R_{ij} = 0 \Rightarrow R_{ij} = \omega_{ij} \frac{r_i r_j}{\rho_i \rho_j} N_{ij} \quad (\text{S19})$$

$$N_{ij}^{\&} = -r_i N_{ij} + \rho_i R_i - r_j N_{ij} + \rho_j R_j - a_{ij} N_{ij} + \alpha_{ij} A_{ij} = 0 \quad (\text{S20})$$

$$A_{ij}^{\&} = a_{ij} N_{ij} - \alpha_{ij} A_{ij} = 0 \Rightarrow A_{ij} = \frac{a_{ij}}{\alpha_{ij}} N_{ij} \quad (\text{S21})$$

$$R_{ij} + R_j + R_i + N_{ij} + A_{ij} = 1 \quad (\text{S22})$$

$$P_{ij} = \frac{p}{\pi \mu} \left(\frac{a_{ij}}{\alpha_{ij}} + \frac{\lambda_i r_i}{\rho_i} + \frac{\lambda_j r_j}{\rho_j} + \frac{\lambda_{ij} \omega_{ij} r_i r_j}{\rho_i \rho_j} \right) / \left(\omega_{ij} \frac{r_i r_j}{\rho_i \rho_j} + \frac{r_j}{\rho_j} + \frac{r_i}{\rho_i} + 1 + \frac{a_{ij}}{\alpha_{ij}} \right) \quad (\text{S23})$$

$$\lambda_{ij}(I) = \Lambda_{ij}(1 + L_{ij}I) \quad (\text{S24})$$

$$P_{ij}^{\max} = \frac{p}{\pi} \frac{m_{ij}}{\mu} \frac{a_{ij}}{\alpha_{ij}} / \left(1 + \frac{a_{ij}}{\alpha_{ij}} \right); P_{ij}^{\min} = \frac{p}{\pi \mu} \Lambda_{ij} \quad (\text{S25})$$

$$P_i = \frac{P_{ij}^{\max} \left(1 + \frac{a_{ij}}{\alpha_{ij}}\right) + \frac{p}{\pi\mu} \left(\frac{\lambda_i r_i}{\rho_i} + \frac{\lambda_j r_j}{\rho_j}\right) + P_{ij}^{\min} \frac{\lambda_{ij}}{\Lambda_{ij}} \frac{\omega_{ij} r_i r_j}{\rho_i \rho_j}}{\frac{r_i}{\rho_i} + \frac{r_j}{\rho_j} + \frac{\omega_{ij} r_i r_j}{\rho_i \rho_j} + u_{ij}} \quad (\text{S26})$$

$$P_i = \frac{P_{ij}^{\max} \left(1 + \frac{a_{ij}}{\alpha_{ij}}\right) + P_i^{\min} \frac{k_i^+ (1 + L_i I)}{k_i^- I^{n_i} f_i(I)} + P_j^{\min} \frac{k_j^+ (1 + L_j I)}{k_j^- I^{n_j} f_j(I)} + P_{ij}^{\min} \frac{\omega_{ij} k_i^+ k_j^+ (1 + L_{ij} I)}{k_i^- k_j^- I^{n_i+n_j} f_i(I) f_j(I)}}{\frac{k_i^+}{k_i^- I^{n_i} f_i(I)} + \frac{k_j^+}{k_j^- I^{n_j} f_j(I)} + \frac{\omega_{ij} k_i^+ k_j^+}{k_i^- k_j^- I^{n_i+n_j} f_i(I) f_j(I)} + u_{ij}} \quad (\text{S27})$$

$$v_{ij} = n_i + n_j \sqrt{\left(1 + \frac{a_{ij}}{\alpha_{ij}}\right) \frac{k_i^- k_j^-}{k_i^+ k_j^+}}$$

$$P_{ij} = \frac{P_{ij}^{\max} (v_{ij} I)^{n_i+n_j} f^2(I) + \left[P_i^{\min} (1 + L_i I) \frac{(v_j I)^{n_j}}{u_j} + P_j^{\min} (1 + L_j I) \frac{(v_i I)^{n_i}}{u_i} \right] f(I) + \omega_{ij} P_{ij}^{\min} (1 + L_{ij} I)}{(v_{ij} I)^{n_i+n_j} f^2(I) + \left[\frac{(v_i I)^{n_i}}{u_i} + \frac{(v_j I)^{n_j}}{u_j} \right] f(I) + \omega_{ij}}$$

The interaction parameter ω_j accounts for a possible stabilization ($\omega_j > 1$) or destabilization ($\omega_j < 1$) of repressors bound to the promoter D_{ij} . If the repressors bind to the promoter independently, $\omega_j = 1$; while if they prevent each other from binding to the promoter, $\omega_j = 0$. Values $\omega_j < 0$ might indicate the existence of additional transitions between promoter states, or the failure of the detailed balance assumption.

Similar to the double operator-containing promoters, we developed a more detailed model for the triple operator-containing promoter, replacing the repressed state R by seven different states (Fig. S4).

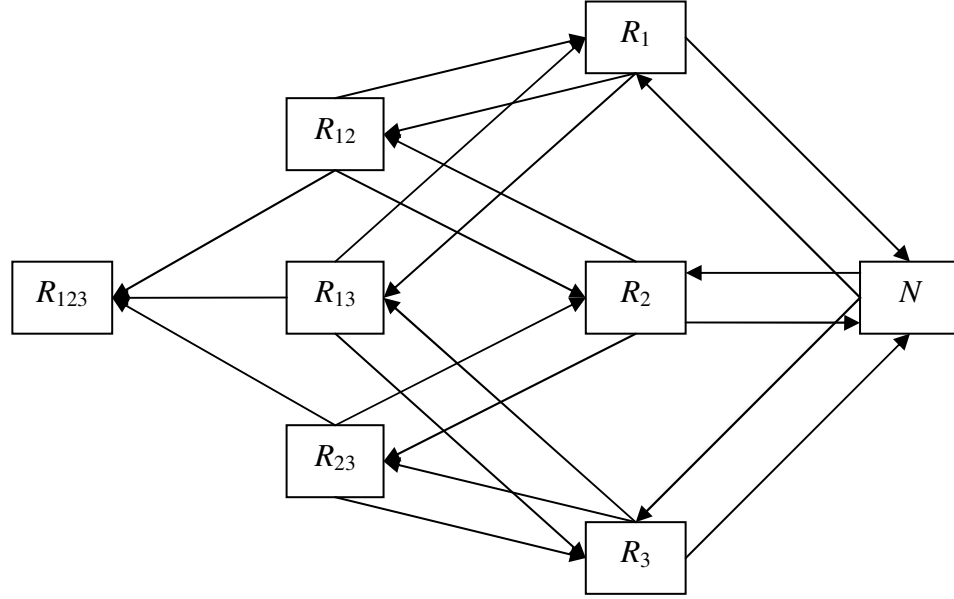


Figure S4: Repressed states for modeling the triple operator-containing promoter T123.

Following a similar line of calculations as for the double operator-containing promoters, we obtain for promoter T123:

$$\begin{aligned}
 P_{123} = & \frac{P_{123}^{\max} (v_{123} I)^{n_1+n_2+n_3} f^3(I) + \sum \left[P_i^{\min} (1+L_i I) \frac{(v_{jk} I)^{n_j+n_k}}{1 + \frac{a_{jk}}{\alpha_{jk}}} \right] f^2(I)}{(v_{123} I)^{n_1+n_2+n_3} f^3(I) + \sum \left[\frac{(v_{ij} I)^{n_i+n_j}}{1 + \frac{a_{ij}}{\alpha_{ij}}} \right] f^2(I) + \sum \left[\omega_{ij} \frac{(v_i I)^{n_k}}{1 + \frac{a_k}{\alpha_k}} \right] f(I) + \omega_{123}} + \\
 & + \frac{\sum \left[P_{ij}^{\min} \omega_{ij} (1+L_{ij} I) \frac{(v_k I)^{n_k}}{1 + \frac{a_k}{\alpha_k}} \right] f(I) + P_{123}^{\min} \omega_{123} (1+L_{123} I)}{(v_{123} I)^{n_1+n_2+n_3} f^3(I) + \sum \left[\frac{(v_{ij} I)^{n_i+n_j}}{1 + \frac{a_{ij}}{\alpha_{ij}}} \right] f^2(I) + \sum \left[\omega_{ij} \frac{(v_i I)^{n_k}}{1 + \frac{a_k}{\alpha_k}} \right] f(I) + \omega_{123}}
 \end{aligned}$$

Assuming independent binding of repressors to their sites ($\omega_{12} = \omega_{13} = \omega_{23} = \omega_{123} = 1$), we estimated the parameters L_{12} ($= -0.0023$), L_{13} ($= 0.079$), L_{23} ($= 0.042$), and L_{123} ($= 0.498$), and used the resulting chemical reaction scheme to calculate the noise as in the generic model (Fig. S1). The unrealistic, negative value of the parameter L_{12} suggests a decrease in basal expression as the inducer concentration increases, and causes the unusual shape of the theoretical induction curve for the triple operator-containing promoter (Fig. S5). Forcing the parameter L_{12} to take only non-negative values yields $L_{12} = 0$, and improves the shape of the theoretical dose-response curve of the T123 promoter (results not shown). The distances between the experimental data and the theoretical fit increased compared to the generic model; they increased to 0.6220, 0.6912, 0.3923, and 2.3398 for promoters D12, D13, D23 and T123, respectively. Taken together, the resulting dose-response curves and noise (Fig. S5) indicate that the behavior of multiple operator-containing promoters cannot be explained by a trivial superposition of independent repressor binding events. This is especially true for the triple-operator containing promoter (Fig. S5), suggesting that promoters with increased number of operator sites are less predictable.

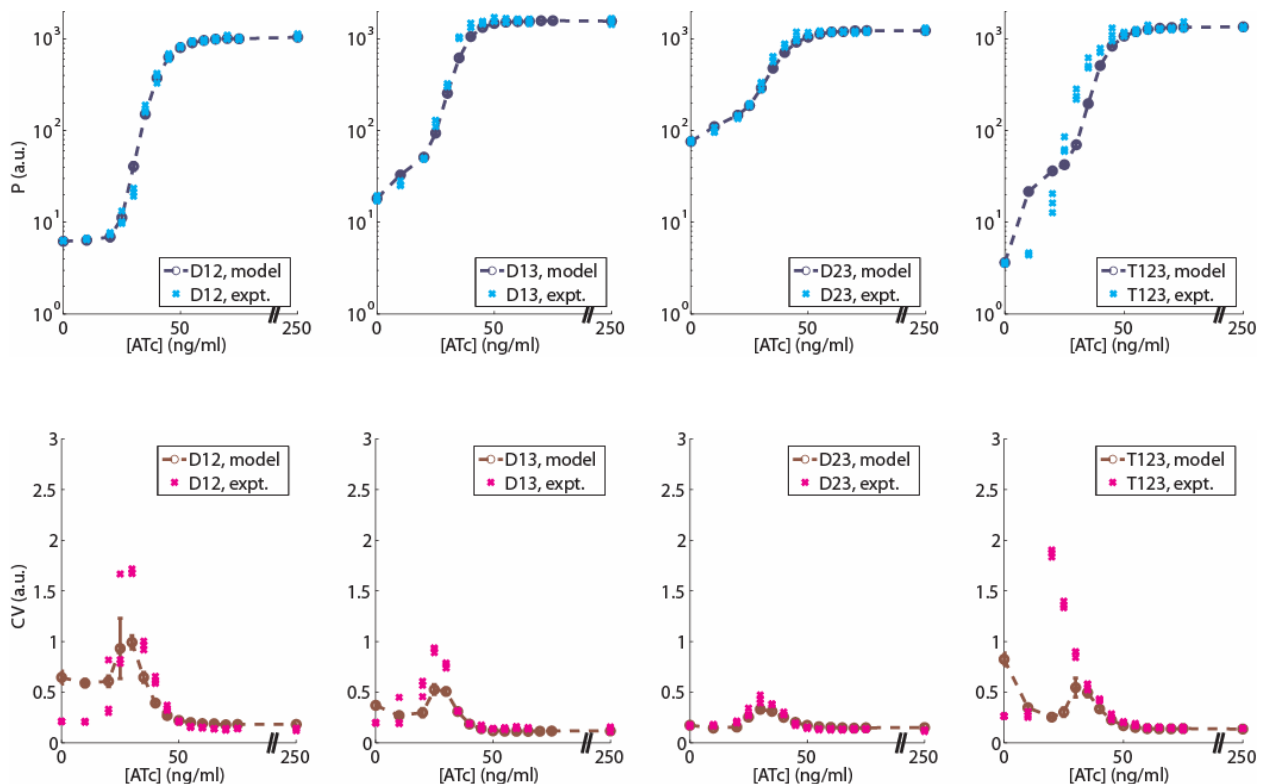


Figure S5: Dose-response curves (top row) and noise (bottom row) for the multiple operator-containing promoters, assuming independent binding of repressors to their operator sites.

Next, to investigate the possibility that repressors might interact on multiple operator-containing promoters, we used nonlinear optimization to estimate the inducer-independent interaction constants ω_{12} , ω_{13} , ω_{23} , and ω_{123} , along with the parameters L_{12} , L_{13} , L_{23} , and L_{123} . All constants except L_{123} were estimated to be positive ($L_{12} = 0.01$, $\omega_{12} = 2.68$, $L_{13} = 0.047$, $\omega_{13} = 0.36$, $L_{23} = 0.033$, $\omega_{23} = 0.53$, $L_{123} = -0.065$, and $\omega_{123} = 0.004$), indicating that repressors de-stabilize each other on promoters D13 and D23, while they stabilize each other on promoter D12. We forced L_{123} to take non-negative values only, and obtained $L_{123} = 0$ and $\omega_{123} = 0.004$. As the plots in Fig. S6 indicate, the assumption of inducer-independent interactions between repressors improves the agreement between the experiment and the simulation, but it is still insufficient to capture the full behavior of multiple operator-containing promoters.

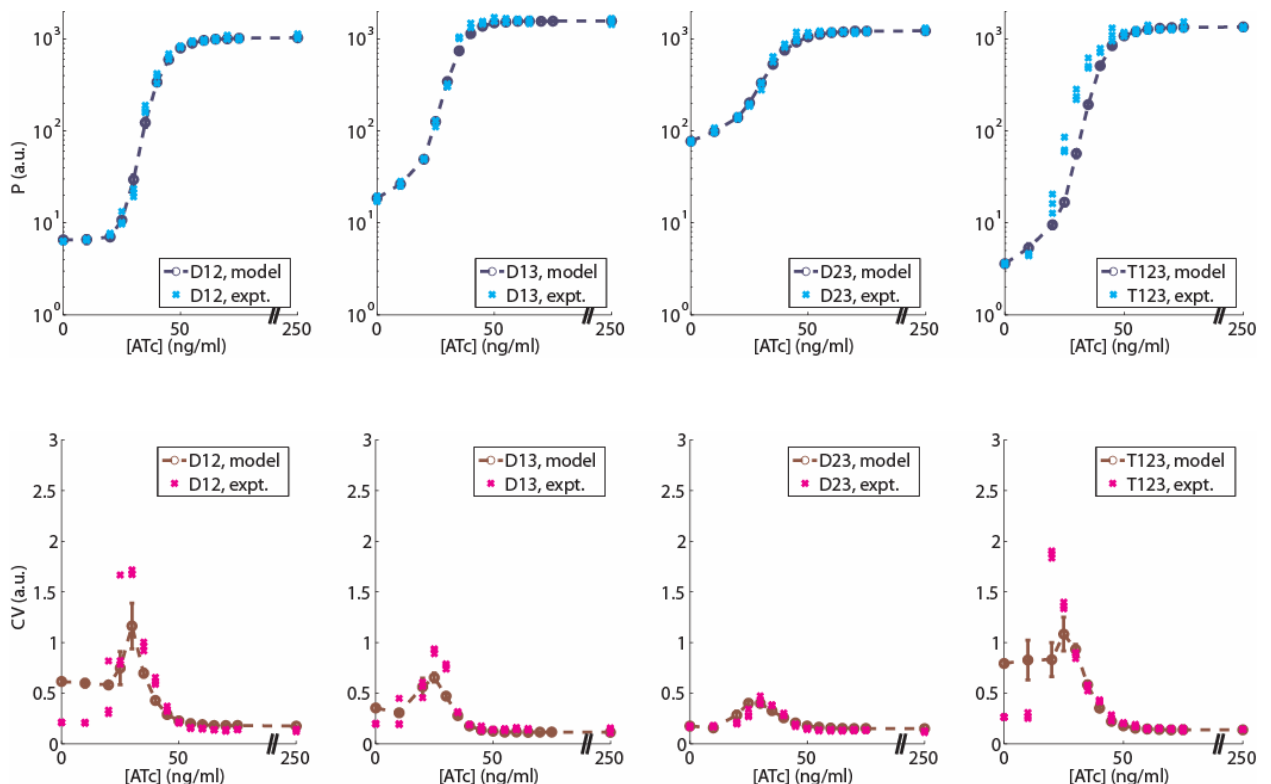


Figure S6: Dose-response curves (top row) and noise (bottom row) for the multiple operator-containing promoters, assuming inducer-independent interactions between repressors.

Finally, we studied if the repressor-dependent interaction functions $\omega_{12}(I)$, $\omega_{13}(I)$, $\omega_{23}(I)$, and $\omega_{123}(I)$ can be calculated analytically, given the parameters of the generic model that assumes a single repressed state for all promoters (Fig. S1). The dose-response function of the promoter D_{ij} can be expressed either based on the detailed (Fig. S3) or the generic (Fig. S1) model, respectively, implying the equality

$$\tilde{P}_{ij} = \frac{p \left(\frac{ma_{ij}}{\alpha_{ij}} + \frac{\lambda_i r_i}{\rho_i} + \frac{\lambda_j r_j}{\rho_j} + \frac{\tilde{\lambda}_{ij} \omega_{ij} r_i r_j}{\rho_i \rho_j} \right)}{\frac{r_i}{\rho_i} + \frac{r_j}{\rho_j} + \frac{\omega_{ij} r_i r_j}{\rho_i \rho_j} + 1 + \frac{a_{ij}}{\alpha_{ij}}} = \frac{p \left(\frac{ma_{ij}}{\alpha_{ij}} + \frac{\lambda_{ij} r_{ij}}{\rho_{ij}} \right)}{\frac{r_{ij}}{\rho_{ij}} + 1 + \frac{a_{ij}}{\alpha_{ij}}} = P_{ij}. \quad (\text{S31})$$

After some calculations, we obtain for the interaction function $\omega_{ij}(I)$:

$$\omega_{ij}(I) = \frac{\left(\frac{k_i^+}{k_i^- I^{n_i} f(I)} + \frac{k_j^+}{k_j^- I^{n_j} f(I)} + 1 + \frac{a_{ij}}{\alpha_{ij}} \right) \left[\frac{ma_{ij}}{\alpha_{ij}} + \frac{k_{ij}^+ \lambda_{ij}}{k_{ij}^- I^{n_{ij}} f(I)} \right]}{\frac{k_i^+ k_j^+ \tilde{\lambda}_{ij}}{k_i^- k_j^- I^{n_i+n_j} f^2(I)} \left(\frac{k_{ij}^+}{k_{ij}^- I^{n_{ij}} f(I)} + 1 + \frac{a_{ij}}{\alpha_{ij}} \right) - \frac{k_i^+ k_j^+}{k_i^- k_j^- I^{n_i+n_j} f^2(I)} \left(\frac{ma_{ij}}{\alpha_{ij}} + \frac{k_{ij}^+ \lambda_{ij}}{k_{ij}^- I^{n_{ij}} f(I)} \right)}$$

$$\frac{\left(\frac{ma_{ij}}{\alpha_{ij}} + \frac{k_i^+ \lambda_i}{k_i^- I^{n_i} f(I)} + \frac{k_j^+ \lambda_j}{k_j^- I^{n_j} f(I)} \right) \left(\frac{k_{ij}^+}{k_{ij}^- I^{n_{ij}} f(I)} + 1 + \frac{a_{ij}}{\alpha_{ij}} \right)}{\frac{k_i^+ k_j^+ \tilde{\lambda}_{ij}}{k_i^- k_j^- I^{n_i+n_j} f^2(I)} \left(\frac{k_{ij}^+}{k_{ij}^- I^{n_{ij}} f(I)} + 1 + \frac{a_{ij}}{\alpha_{ij}} \right) - \frac{k_i^+ k_j^+}{k_i^- k_j^- I^{n_i+n_j} f^2(I)} \left(\frac{ma_{ij}}{\alpha_{ij}} + \frac{k_{ij}^+ \lambda_{ij}}{k_{ij}^- I^{n_{ij}} f(I)} \right)}$$

As this formula indicates, the interaction functions depend on the basal promoter expression ($\tilde{\lambda}_{ij}$) from the double-repressed state R_{ij} . So far, we considered that the basal promoter expression increases linearly with the inducer concentration. However, this

might be a simplifying assumption, and in reality both $\tilde{\lambda}_{ij}$ and ω_{ij} can depend on the inducer concentration in a non-trivial way. The current experimental technology is not capable of measuring these parameters independently. Therefore, in the most general sense, the predictability of multiple operator-containing promoters remains challenging to answer completely.

6. The effect of promoter sequence changes on pretranscriptional events

All eight promoters (WT, S1, S2, S3, D12, D13, D23, and T123) have different expression levels at full induction (see Table S2). To determine if these differences were due to the replacement of native *GALI* promoter sequences with the *tetO₂* operators, we replaced the operator site in the S2 promoter with two random sequences. One of these sequences (S2-P) was palindromic (similar to the *tetO₂* operator site), while the other (S2-R) was random (Fig. S7 *Upper*). Both of these sequences caused large decreases in gene expression (see Fig. S7 *Lower*), indicating that the *GALI* promoter sequence in this region plays a role in promoter activity, and alterations can lead to lower maximal expression. Additional controls involving a premature stop codon in the *tetR* coding sequence further indicated that residual repressor binding could not account for these differences. Thus, we hypothesized that the insertion of operator sites alters the efficiency of various events that precede transcription initiation, such as general transcription factor binding and PIC assembly, RNA polymerase II binding, or DNA melting.

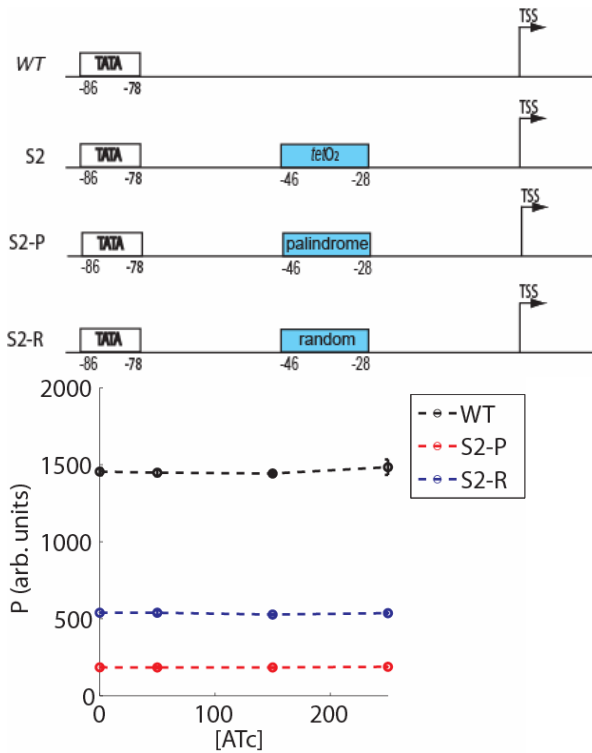


Figure S7: Promoter constructs to test the effect of sequence changes on transcription initiation (*Upper*) and the observed changes in gene expression (*Lower*). The average gene expression from promoter S2 (not shown here) is 855 ± 10 .

To model the effect of promoter sequence changes, we assumed the events that precede transcription initiation occur sequentially along the promoter, starting from the TATA box and propagating toward the transcription START site. Therefore, we replaced the transitions between promoter states N and A in Fig. S1 with a more detailed reaction scheme comprising three different stages of promoter activation: A, B, and C (Fig. S8). We also assumed that the insertion of repressor sites into promoters S1, S2 and S3 independently affect the transition rates $N \leftrightarrow A$, $A \leftrightarrow B$, and $B \leftrightarrow C$, respectively.

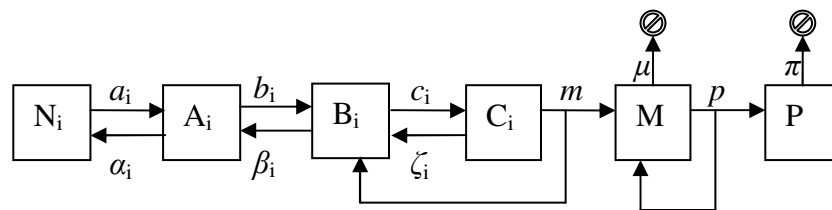


Figure S8: Detailed reaction scheme for modeling the effect of repressor sites on the maximum expression levels from all eight promoters.

Using chemical mass action kinetics and assuming detailed balance, we estimated the maximum expression levels from various promoters as follows:

$$N_i^{\&} = -a_i N_i + \alpha_i A_i = 0 \Rightarrow A_i = \frac{a_i}{\alpha_i} N_i \quad (\text{S33})$$

$$A_i^{\&} = a_i N_i - \alpha_i A_i - b_i A_i + \beta_i B_i \quad (\text{S34})$$

$$B_i^{\&} = b_i A_i - \beta_i B_i - c_i B_i + \zeta_i C_i + m C_i \Rightarrow B_i = \frac{b_i}{\beta_i} A_i = \frac{b_i}{\beta_i} \frac{a_i}{\alpha_i} N_i \quad (\text{S35})$$

$$C_i^{\&} = c_i B_i - \zeta_i C_i - m C_i \Rightarrow C_i = \frac{c_i}{\zeta_i + m} B_i = \frac{c_i}{\zeta_i + m} \frac{b_i}{\beta_i} \frac{a_i}{\alpha_i} N_i \quad (\text{S36})$$

$$N_i + A_i + B_i + C_i = 1 \quad (\text{S37})$$

$$N_i = \frac{1}{1 + \frac{a_i}{\alpha_i} + \frac{a_i}{\alpha_i} \frac{b_i}{\beta_i} + \frac{b_i}{\beta_i} \frac{a_i}{\alpha_i} \frac{c_i}{\zeta_i + m}} \quad (\text{S38})$$

$$M_i^{\&} = m C_i - \mu M_i = 0 \Rightarrow M_i = \frac{m}{\mu} C_i = \frac{\frac{b_i}{\beta_i} \frac{a_i}{\alpha_i} \frac{c_i}{\zeta_i + m} \frac{m}{\mu}}{1 + \frac{a_i}{\alpha_i} + \frac{a_i}{\alpha_i} \frac{b_i}{\beta_i} + \frac{b_i}{\beta_i} \frac{a_i}{\alpha_i} \frac{c_i}{\zeta_i + m}} \quad (\text{S39})$$

$$P_i = \frac{p}{\pi} M_i = \frac{p}{\pi\mu} \frac{\frac{b_i}{\beta_i} \frac{a_i}{\alpha_i} \frac{c_i m}{\zeta_i + m}}{\left(1 + \frac{a_i}{\alpha_i} + \frac{b_i}{\beta_i} \frac{a_i}{\alpha_i} + \frac{b_i}{\beta_i} \frac{a_i}{\alpha_i} \frac{c_i}{\zeta_i + m}\right)} = \frac{p}{\pi\mu} \frac{m}{\frac{\alpha_i}{a_i} \frac{\beta_i}{b_i} \frac{\zeta_i + m}{c_i m} + \frac{\beta_i}{b_i} \frac{\zeta_i + m}{c_i m} + \frac{\zeta_i + m}{c_i m} + 1}$$

$$\frac{p}{\pi\mu} \frac{1}{P_i} = \frac{1}{m} \left(\frac{\alpha_i}{a_i} \frac{\beta_i}{b_i} \frac{\zeta_i + m}{c_i m} + \frac{\beta_i}{b_i} \frac{\zeta_i + m}{c_i m} + \frac{\zeta_i + m}{c_i m} + 1 \right). \quad (\text{S40})$$

Introducing the notation

$$x_1, y_1 \propto \frac{\alpha_i}{a_i}; x_2, y_2 \propto \frac{\beta_i}{b_i}; x_3, y_3 \propto \frac{\zeta_i + m}{c_i}; x_3, z \propto \frac{1}{m}; N = \frac{p}{\pi\mu}, \quad (\text{S41})$$

we obtain the system of algebraic equations

$$\begin{cases} y_1 x_2 x_3 z + x_2 x_3 z + x_3 z + z = NP_1^{-1} \\ x_1 y_2 x_3 z + y_2 x_3 z + x_3 z + z = NP_2^{-1} \\ y_1 x_2 y_3 z + x_2 y_3 z + y_3 z + z = NP_3^{-1} \\ y_1 y_2 x_3 z + y_2 x_3 z + x_3 z + z = NP_{12}^{-1} \\ y_1 x_2 y_3 z + x_2 y_3 z + y_3 z + z = NP_{13}^{-1} \\ x_1 y_2 y_3 z + y_2 y_3 z + y_3 z + z = NP_{23}^{-1} \\ y_1 y_2 y_3 z + y_2 y_3 z + y_3 z + z = NP_{123}^{-1} \\ x_1 x_2 x_3 z + x_2 x_3 z + x_3 z + z = NP_0^{-1} \end{cases} \quad (\text{S42})$$

This appears to be an over-determined system of eight equations and seven unknowns.

However, when we select subsets of seven equations, the resulting systems contain variables that depend on each other, and therefore explicit solutions cannot be found.

Thus, we used the Symbolic Math Toolbox (Matlab by the Mathworks, Inc.) to determine an implicit solution (all unknowns as functions of x_1) from six equations.

Next, we calculated the explicit solutions (consisting of all seven unknowns) by scanning the values of x_1 over 20 orders of magnitude (from 10^{-10} to 10^{10}). Surprisingly, the value of at least one unknown was always negative, which is unrealistic, because all unknowns correspond to chemical equilibrium constants. Therefore we reasoned that the mean maximum expression values on the right-hand side must be affected by experimental error.

We took into account the variation of maximum expression levels between different experiments, and solved the system of equations repeatedly after altering the maximum expression values by a Monte-Carlo technique. In this search for positive solutions, we selected the maximum expression values from a Gaussian distribution with the experimental mean and standard deviation. We accepted only positive solutions while minimizing the Euclidian distance between the altered and mean maximum expression values. The results of 50 successful trials can be seen in Figs. S9-S11.

Several conclusions can be drawn from Figs. S9-S11. First, Fig. S9 allows the theoretical estimation of experimental errors. For example, for promoter D13, the successful trials result in consistently higher values of estimated maximum expression (circles) than the experimental mean (dashed line). The opposite is true for gene expression from the wild-type (WT) promoter, for which the theoretically estimated maximum expression values tend to be consistently lower than the experimental mean.

Fig. S10 indicates that the solutions can vary over many orders of magnitude. Strong correlations and anti-correlations exist between some pairs of unknowns (for example, x_1 and y_1 are strongly correlated, while x_1 and x_2 are strongly anti-correlated). Also, x_1 and y_1 are consistently lower, while x_2 and y_2 are consistently higher than all other solutions. Taken together with the definition of these variables, this suggests that the rate-limiting step during preinitiation is some reaction affected by the insertion of the operator site in promoter S2, while the insertion of operator sites into S1 and S3 had a much lower overall effect.

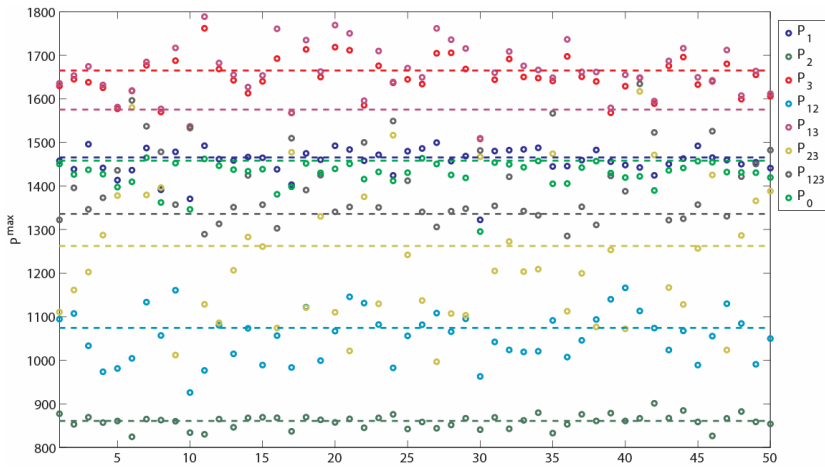


Figure S9: Maximum expression values from 50 successful trials. Dashed lines represent the experimental means.

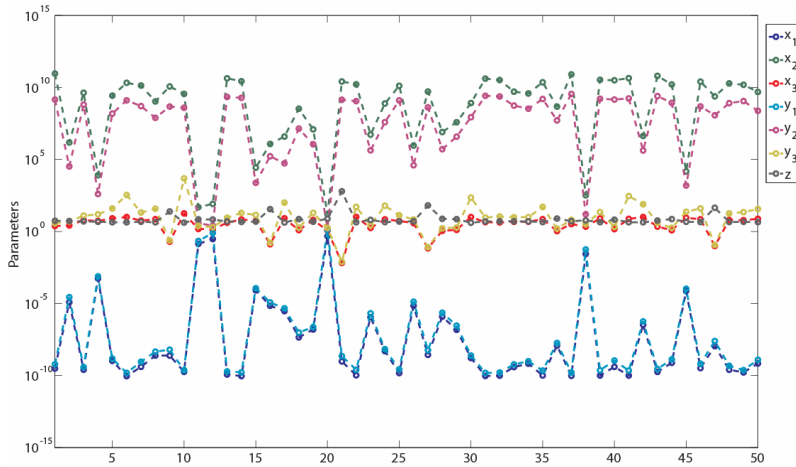


Figure S10: Solutions of the system of equations from 50 successful trials.

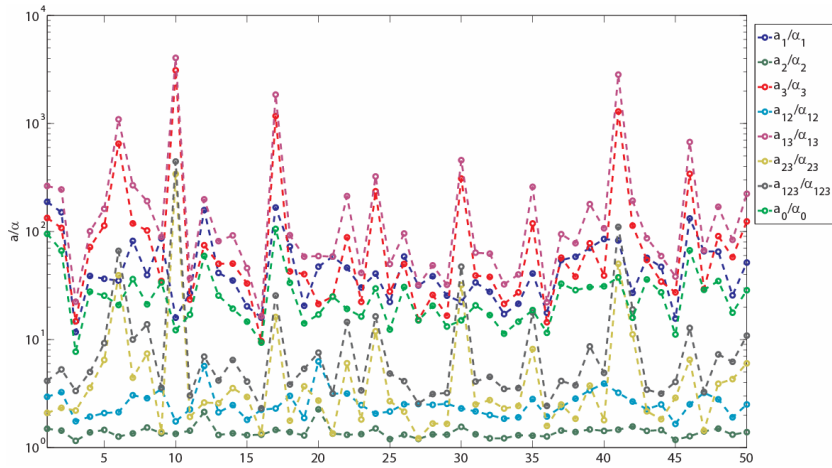


Figure S11: Equilibrium constants for $N \leftrightarrow A$ in the generic model for 50 successful trials.

Finally, Fig. S11 allows us to estimate the promoter activity for all eight promoters, characterized by the equilibrium constant for transitions between the states N and A in our generic model, equal to a/α in Fig. S1. Despite the large variations in the graph, Fig S10 indicates that promoters S1, S3 and D13 clearly have the highest promoter activity, as reflected by their expression levels at full induction (Fig. S9 and Table S2).

7. Independent control of the mean and noise in gene expression

Several current studies indicate the phenotypic importance of gene expression noise (9, 10). To verify the phenotypic consequences of promoter-mediated transcriptional noise (10), it is important to establish conditions where two cell populations possess the same average gene expression, but different degrees of cell-cell variability. Typically, altering cellular components to change the noise also causes a change in the mean. Therefore, it becomes important to modify the noise and the mean of gene expression independently of each other, thereby separating their effects on the population's phenotype. As indicated by Fig. S12, our seven promoters permit the establishment of conditions where two cell populations have the same mean, but different noise.

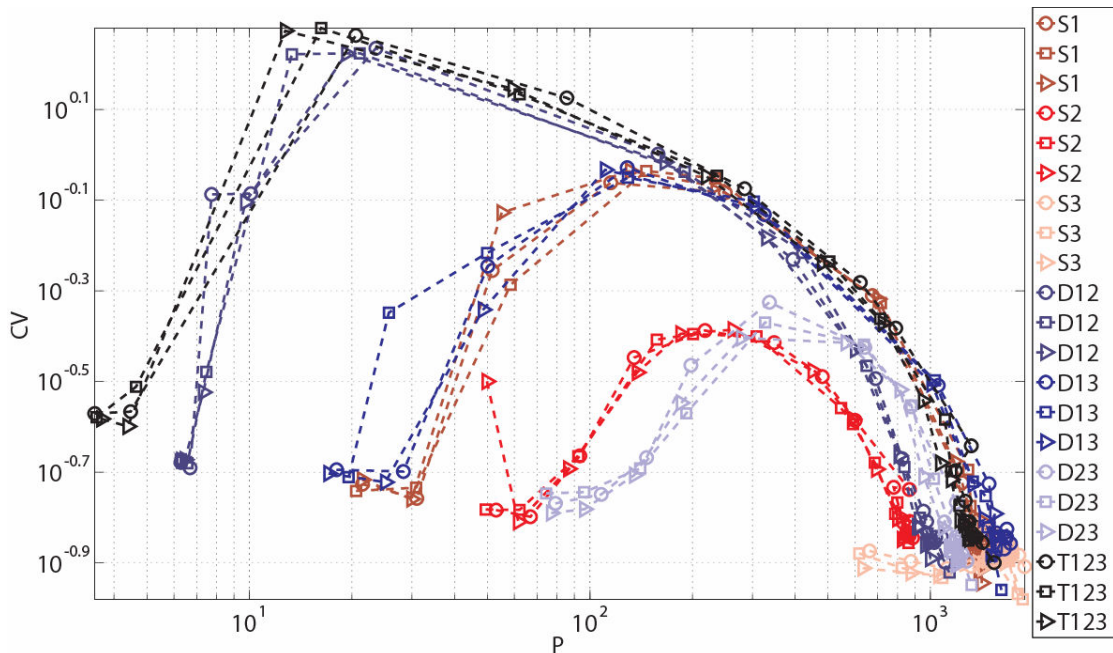


Figure S12: Coefficient of variation (CV) as a function of mean for all seven engineered promoters.

8. The effect of autofluorescence on noise

We measured the autofluorescence experimentally in the untransformed parent strain YPH500, which lacks *yEGFP*. YPH500 cultures were grown and assayed as described in the main text, and included 0-250 ng/ml ATc. Taking into account the existence of autofluorescence ($P = 2.7 \pm 0.3$), we re-estimated our parameters and re-ran our stochastic simulations to quantify the effect of this experimental factor on our modeling results. As Fig. S13 indicates, taking autofluorescence into account improves the agreement between model and experiment at low induction levels (near $[ATc] = 0$), especially for the promoters with high repression efficiency (promoters S1, D12, and T123). On the other hand, for promoters with high basal expression (S2, S3, S23), promoter leakage overshadows the contribution of background autofluorescence. The combined effect of promoter leakage and autofluorescence background causes the existence of a noise peak at intermediate levels of induction. As shown previously, if both

promoter leakage and autofluorescence were absent, the noise would continue to increase as we approach $[ATc] = 0$, and the noise peak would be absent.

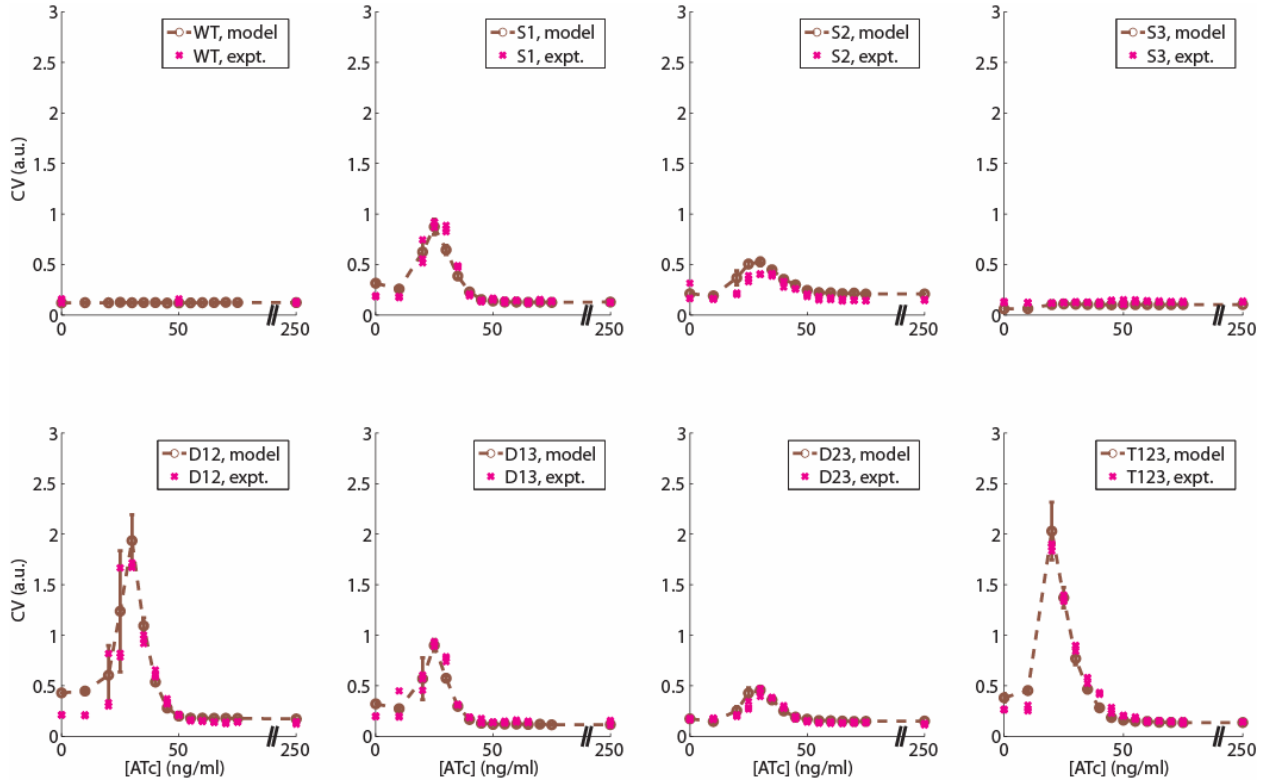


Figure S13: Coefficient of variation (CV) for all seven engineered promoters, after taking into account the autofluorescence. Compare with Fig. 4 in the main text.

9. The effect of parameters on noise

We varied several parameters (p , π , m , μ , s_A , s_R) in our generic model to determine their effect on the noise as a function of inducer concentration. As shown in Fig. S14, all of these parameters affect noise intensity. Increasing the protein or mRNA synthesis rates (p or m) results in increased noise intensity at all induction levels. Increasing the mRNA half-life (t_M) has a similar effect. Interestingly, while increasing the protein half-life (t_P) causes an increase in noise only at high levels of induction, it causes a decrease in noise intensity at intermediate levels of induction, probably indicating that slow protein degradation acts as a filter that diminishes the high end of the noise spectrum. Finally,

increasing either of the scaling factors, s_A or s_R , causes a decrease in noise intensity. High values for these scaling factors correspond to fast transitions between promoter states, which shift gene expression noise toward the high-frequency regime of the spectrum. This regime is filtered out by slow protein decay, leading to lower total noise intensity.

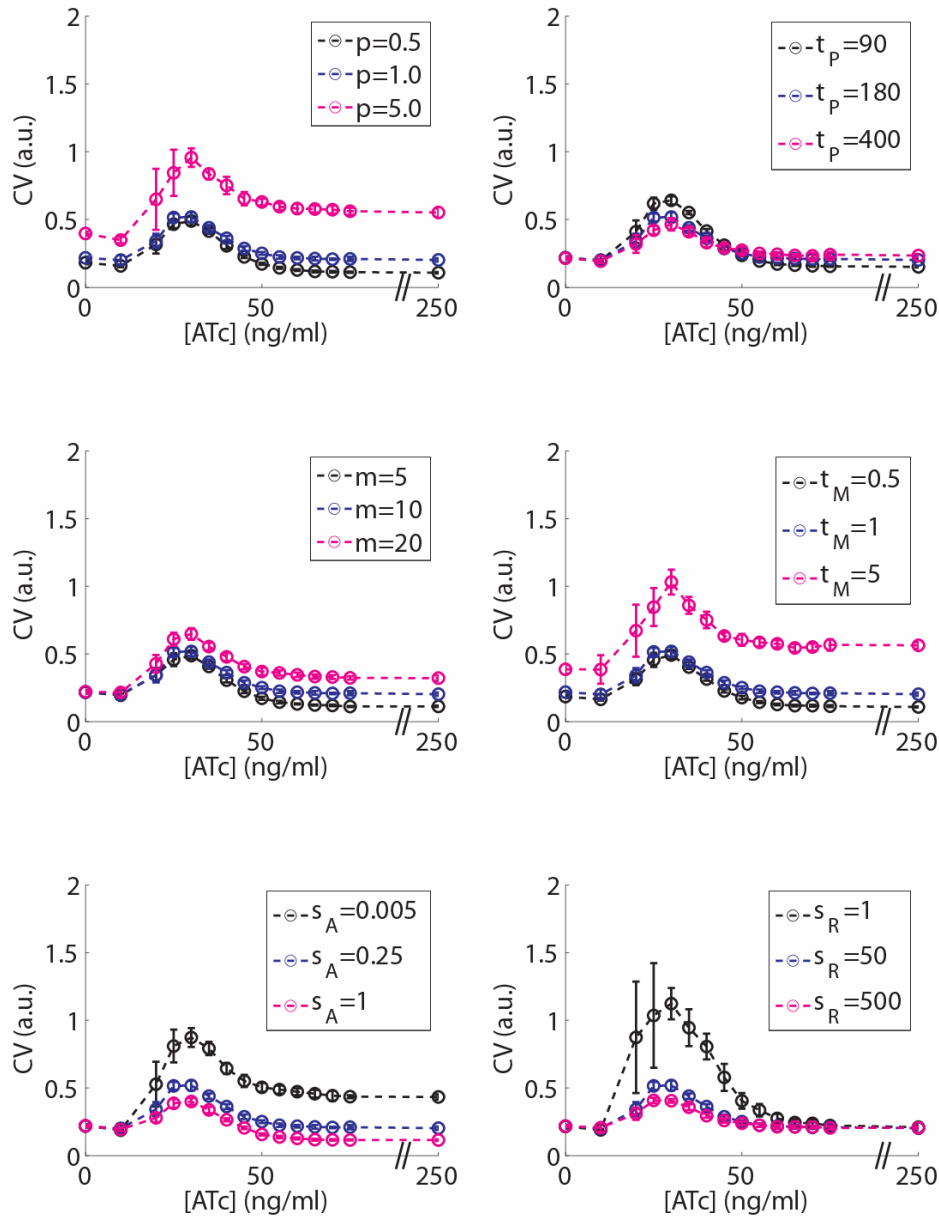


Figure S14: The effect of various parameters (p , π , m , μ , s_A , s_R) on noise intensity.

10. Fitting the the experimental data by the Hill function

As described in the main text, we initially fit our data by the Hill function:

$$P(I) = P_{\min} + (P^{\max} - P^{\min}) \frac{I^h}{H^h + I^h}.$$

The parameters H (induction threshold) and h (steepness of response or Hill coefficient) that we obtained from this fit are listed in Table S2.

	WT	S1	S2	S3	D12	D13	D23	T123
P^{\max}	1458±25	1461±22	855±10	1694±33	1039±64	1565±124	1235±68	1357±29
P^{\min}	1458±25	21.2±0.5	50±2	637±22	6.29±0.01	18±1.2	76±2.4	3.58±0.09
H	N/A	36.42	39.17	18.33	42.22	34.63	36.79	37.31
h	N/A	6.67	4.82	2.74	11.13	7.71	5.49	7.38

Table S2: Parameters estimated by fitting the Hill function to our experimental data.

As shown in Fig. S15, the empirical Hill function did not fit our data well, especially at low levels of induction. Therefore, we moved on to the chemical reaction scheme, as described in the main text.

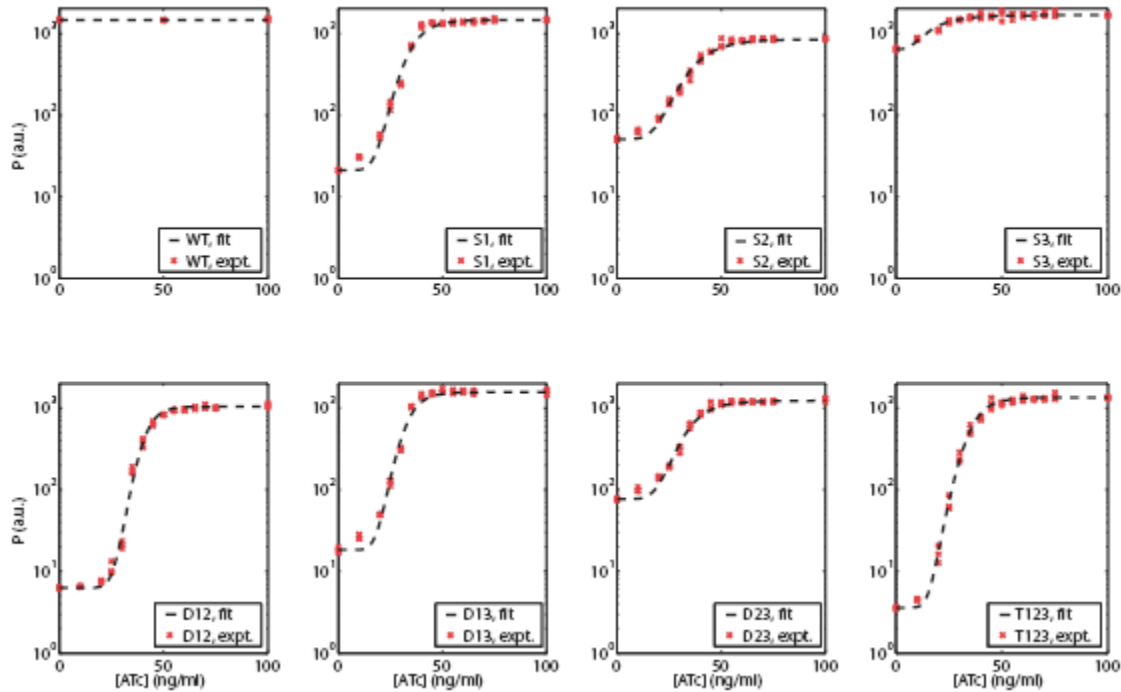


Figure S15: Hill functions (dashed black lines) fitted to our experimental data (red crosses).

1. Blake WJ, M, KA, Cantor CR, Collins JJ (2003) *Nature* 422:633-637.
2. Berens C, Hillen W (2003) *Eur J Biochem* 270:3109-3121.
3. Garcia-Martinez J, Aranda A, Perez-Ortin JE (2004) *Mol Cell* 15:303-313.
4. Hoopes BC, LeBlanc JF, Hawley DK (1998) *J Mol Biol* 277:1015-1031.
5. Bryant GO, Ptashne M (2003) *Mol Cell* 11:1301-1309.
6. Johnston GC, Ehrhardt CW, Lorincz A, Carter BL (1979) *J Bacteriol* 137:1-5.
7. Gillespie DT (1977) *J Phys Chem* 81:2340-2361.
8. Ramsey S, Orrell D, Bolouri H (2005) *J Bioinform Comput Biol* 3:415-436.
9. Becskei A, Kaufmann BB, van Oudenaarden A (2005) *Nat Genet* 37:937-944.
10. Blake WJ, Balazsi G, Kohanski MA, Isaacs FJ, Murphy KF, Kuang Y, Cantor CR, Walt DR, Collins JJ (2006) *Mol Cell* 24:853-865.